

Research Article

Zakaria Belhachmi, Thomas Glatz* and Otmar Scherzer

Photoacoustic tomography with spatially varying compressibility and density

DOI: 10.1515/jiip-2015-0113

Received December 23, 2015; revised July 8, 2016; accepted September 8, 2016

Abstract: This paper investigates photoacoustic tomography with two spatially varying acoustic parameters, the compressibility and the density. We consider the reconstruction of the absorption density parameter (imaging parameter of Photoacoustics) with complete and partial measurement data. We investigate and analyze three different numerical methods for solving the imaging problem and compare the results.

Keywords: Photoacoustic imaging, spatially varying compressibility and density, variable sound speed, regularization, time reversal

MSC 2010: 65J22, 35R30

1 Introduction

Photoacoustic Imaging (PAI) is a novel technique for tomographical imaging of small biological or medical specimens. The method makes use of the fact that an object expands after being exposed to ultrashort electromagnetic radiation, and emits an ultrasonic wave (see e.g. [28, 32]). The resulting acoustic pressure is assumed to be proportional to the electromagnetic *absorption*, which is the imaging parameter of Photoacoustics. It provides detailed anatomical and functional information.

Opposed to the conventional photoacoustic imaging [28, 32], which is based on the assumption that the *compressibility* and *density* of the medium are constant (and thus in turn the sound speed), this paper assumes *both* of these parameters spatially varying. The mathematical model describing the propagation of the ultrasonic pressure considered here is

$$\begin{aligned} \kappa(x)y''(x, t) - \nabla \cdot (\rho(x)^{-1}\nabla y(x, t)) &= 0 && \text{in } \mathbb{R}^n \times (0, \infty), \\ y(x, 0) &= f(x) && \text{in } \mathbb{R}^n, \\ y'(x, 0) &= 0 && \text{in } \mathbb{R}^n. \end{aligned} \quad (1.1)$$

Here, κ is the material compressibility, ρ denotes the density and f denotes the amount of absorbed energy, i.e. the imaging parameter that encodes the material properties of physiological interest in PAI. We emphasize that the speed of sound is given by $c(x) = \frac{1}{\sqrt{\kappa\rho}}$ and that this equation is more general than

$$\begin{aligned} y''(x, t) - c^2(x)\Delta y(x, t) &= 0 && \text{in } \mathbb{R}^n \times (0, \infty), \\ y(x, 0) &= f(x) && \text{in } \mathbb{R}^n, \\ y'(x, 0) &= 0 && \text{in } \mathbb{R}^n, \end{aligned} \quad (1.2)$$

Zakaria Belhachmi: Laboratoire de Mathématiques LMIA, Université de Haute Alsace, 4, rue des Frères Lumière, 68200 Mulhouse, France, e-mail: zakaria.belhachmi@uha.fr

***Corresponding author: Thomas Glatz:** Computational Science Center, University of Vienna, Oskar-Morgenstern Platz 1, A-1090 Vienna, Austria, e-mail: thomas.glatz@univie.ac.at

Otmar Scherzer: Computational Science Center, University of Vienna, Oskar-Morgenstern Platz 1, A-1090 Vienna, Austria; and Johann Radon Institute for Computational and Applied Mathematics (RICAM), Austrian Academy of Sciences, Altenbergerstraße 69, A-4040 Linz, Austria, e-mail: otmar.scherzer@univie.ac.at

which also describes acoustic wave propagation in the case of variable sound speed. The latter equation is derived from equation (1.1) under the additional assumption that ρ is spatially slowly varying. Another common approximation is obtained by the assumption that κ is spatially slowly varying and results in

$$\begin{aligned} y''(x, t) - \nabla \cdot (c^2(x)\nabla y(x, t)) &= 0 && \text{in } \mathbb{R}^n \times (0, \infty), \\ y(x, 0) &= f(x) && \text{in } \mathbb{R}^n, \\ y'(x, 0) &= 0 && \text{in } \mathbb{R}^n. \end{aligned} \quad (1.3)$$

For further details on the derivation of equation (1.1) from fluid- and thermodynamics, we refer to [7, Chapter 8.1].

The *photoacoustic reconstruction* consists in determining the function f from measurement data of y on a surface $S \subseteq \partial\Omega$ over time $(0, T)$.

There exists a huge amount of literature on reconstruction formulas in the case $c \equiv 1$, see for instance [16, 17, 29–31, 33, 34] to name but a few. Time reversal in the case of variable sound speed has been studied for instance in [2, 14, 15, 19, 21, 26]. Time reversal for photoacoustic imaging based on equation (1.1) as well as on equation (1.2) has been given in [21] – note that both associated wave operators are special cases of the general operator from [21]. Their theory has been generalized to the elastic wave equation in [24].

In this paper we focus on numerical realization and regularization theory of photoacoustic imaging based on equation (1.1) with different numerical methods. Most closely related to our numerical approach is a time reversal algorithm from [25], which employs the formula equation (3.7) below. Recently we applied iterative regularization techniques in the case of variable sound speed [6] and compared it with time reversal. The goal here is to generalize time reversal and iterative regularization for photoacoustic imaging in the case of spatially variable density and compressibility. A convergence in the least-squares-sense is thereby guaranteed by standard results from regularization theory (see e.g. [8, 10]).

The paper is organized as follows: In Section 2 we analyze the mathematical equations describing wave propagation in the case of spatially variable compressibility and density. Imaging based on this model is analyzed in Section 3. Numerical results are presented for three different methods; time reversal, Neumann series, and Landweber iteration in Section 4. The latter two seem to be new for the presented equation. We also investigate the case of partial measurement data.

1.1 Notation

In the beginning we summarize the basic notation, which is used throughout the paper.

In the following, Ω denotes a non-empty, open, bounded and connected domain in \mathbb{R}^n with Lipschitz and piecewise C^1 -boundary $\partial\Omega$. Moreover, $S \subseteq \partial\Omega$ is connected and relatively open. The vector $\mathbf{n}(x)$, with $x \in \partial\Omega$, denotes the outward pointing unit normal vector of Ω . The absorption density f , the compressibility κ and the density ρ are supposed to satisfy:

- $\kappa, \rho \in C^1(\mathbb{R}^n)$ satisfying $0 < \rho_{\min} \leq \rho(x) \leq \rho_{\max}$ and $0 < \kappa_{\min} \leq \kappa(x) \leq \kappa_{\max}$. Define $c_{\max} := (\kappa_{\min}\rho_{\min})^{-1/2}$. Moreover, we assume that κ, ρ are constant in $\mathcal{C}\Omega$, where $\mathcal{C}\Omega$ denotes the complement of Ω , and satisfy $\kappa\rho = 1$ there.
- The absorption density function f has support in Ω : $\text{supp}(f) \subseteq \Omega$.

For the sake of simplicity of notation we omit space and time arguments of functions whenever this is convenient and does not lead to confusions.

We use the following Hilbert spaces:

- We denote

$$L^2(\Omega) = \{\phi \in L^2(\mathbb{R}^n) : \phi \equiv 0 \text{ in } \mathcal{C}\Omega\},$$

with inner product

$$\langle \phi_1, \phi_2 \rangle_{L^2(\Omega)} = \int_{\mathbb{R}^n} \phi_1 \phi_2 \, dx.$$

- For $\hat{\Omega} = \Omega$ or \mathbb{R}^n :
 - Let $H_0^1(\hat{\Omega})$ be the closure of differentiable functions on \mathbb{R}^n with compact support in $\hat{\Omega}$, associated with the non-standard (but equivalent) inner product

$$\langle \phi_1, \phi_2 \rangle_{1;\kappa,\rho} = \int_{\mathbb{R}^n} \kappa \phi_1 \phi_2 + \rho^{-1} \nabla \phi_1 \cdot \nabla \phi_2 \, dx. \quad (1.4)$$

The associated norm is denoted by $\|\phi\|_{1;\kappa,\rho}$.

- The seminorm associated to the inner product

$$\langle \phi_1, \phi_2 \rangle_{1;\rho} = \int_{\mathbb{R}^n} \rho^{-1} \nabla \phi_1 \cdot \nabla \phi_2 \, dx \quad (1.5)$$

is denoted by $|\phi|_{1;\rho}$.

- The norm associated with the inner product

$$\langle \phi_1, \phi_2 \rangle_1 = \int_{\hat{\Omega}} \phi_1 \phi_2 + \nabla \phi_1 \cdot \nabla \phi_2 \, dx$$

is denoted by $\|\phi\|_1$.

- The norms $\|\phi\|_1$ and $\|\phi\|_{1;\kappa,\rho}$ are equivalent. In fact, we have

$$\sqrt{\min\{\kappa_{\min}, \rho_{\max}^{-1}\}} \|\phi\|_1 \leq \|\phi\|_{1;\kappa,\rho} \leq \sqrt{\max\{\kappa_{\max}, \rho_{\min}^{-1}\}} \|\phi\|_1 \quad \text{for all } \phi \in H_0^1(\hat{\Omega}). \quad (1.6)$$

- We denote by $L^2(S)$ the standard Hilbert space of square integrable functions on $\partial\Omega$ with support in S , together with the inner product

$$\langle \phi_1, \phi_2 \rangle_{L^2(S)} = \int_S \phi_1(x) \phi_2(x) \, dS(x),$$

and $L^2(\Sigma)$ denotes the standard Hilbert space of square integrable functions on $\partial\Omega \times (0, T)$ with support in $\Sigma := S \times (0, T)$, together with the inner product

$$\langle \phi_1, \phi_2 \rangle_{L^2(\Sigma)} = \int_0^T \int_S \phi_1(x, t) \phi_2(x, t) \, dS(x) \, dt.$$

The induced norms are denoted by $\|\cdot\|_{L^2(S)}$, $\|\cdot\|_{L^2(\Sigma)}$. Moreover, $C_0^\infty(\Sigma)$ denotes the space of smooth functions with support in Σ .

- The trace operator $\gamma_\Omega : H^1(\mathbb{R}^n) \rightarrow L^2(\partial\Omega)$ restricts functions defined on \mathbb{R}^n onto $\partial\Omega$, respectively. This operator is the composition of the standard trace operator $\gamma : H^1(\Omega) \rightarrow L^2(\partial\Omega)$ and the restriction operator $R : H^1(\mathbb{R}^n) \rightarrow H^1(\Omega)$, which are both bounded [1, Theorem 5.22], and thus itself bounded. We denote

$$\mathbb{C}_\gamma := \|\gamma \circ R\|. \quad (1.7)$$

2 Direct problem of wave propagation

In this section we are analyzing the *wave operator* L mapping the absorption density f onto the solution y of equation (1.1) restricted to Σ :

$$L : H_0^1(\Omega) \rightarrow L^2(\Sigma), \quad f \mapsto y|_\Sigma. \quad (2.1)$$

First, we show that the operator L is bounded. Analogous to [6], we define the total wave energy by

$$E(t; y) := \frac{1}{2} \int_{\mathbb{R}^n} \kappa y'^2 + \rho^{-1} |\nabla y|^2 \, dx. \quad (2.2)$$

The time derivative of E , taking into account equation (1.1), is

$$E'(t; y) = \int_{\mathbb{R}^n} \kappa y'' y' - \nabla \cdot (\rho^{-1} \nabla y) y' dx = 0 \quad \text{for all } t > 0.$$

Consequently,

$$E(t; y) = E(0; y) = \frac{1}{2} \|f\|_{1;\rho}^2 \quad \text{for all } t > 0. \quad (2.3)$$

This, together with equation (2.2) shows that

$$\int_{\mathbb{R}^n} \kappa y'^2 dx \leq \|f\|_{1;\rho}^2 \quad \text{and} \quad \|y(t)\|_{1;\rho} \leq \|f\|_{1;\rho} \quad \text{for all } t > 0. \quad (2.4)$$

A-priori this inequality does not provide a bound for y in the whole \mathbb{R}^n with respect to the standard H^1 -norm. This is provided for instance by the following lemma:

Lemma 2.1. *Let y be the solution of equation (1.1). Then*

$$\|y(t)\|_{1;\kappa,\rho} \leq \mathcal{C}(T) \|f\|_{1;\kappa,\rho} \quad \text{for all } t \in (0, T), \quad (2.5)$$

where

$$\mathcal{C}(T) := \sqrt{\max\{1 + 2T^2, 2\}}.$$

Proof. For arbitrary $\hat{t} \in (0, T)$ it follows from equation (2.4) that

$$\int_{\mathbb{R}^n} \kappa(x) (y(x, t) - y(x, 0))^2 dx = \int_{\mathbb{R}^n} \kappa(x) \left(\int_0^{\hat{t}} y'(x, \hat{t}) d\hat{t} \right)^2 dx \leq \hat{t} \int_0^{\hat{t}} \int_{\mathbb{R}^n} \kappa y'^2 dx d\hat{t} \leq T^2 \|f\|_{1;\rho}^2.$$

With the elementary inequality $(a - b)^2 \geq \frac{1}{2} a^2 - b^2$ it follows that

$$\begin{aligned} \int_{\mathbb{R}^n} \kappa(x) (y(x, t))^2 dx &\leq 2 \int_{\mathbb{R}^n} \kappa(x) (y(x, t) - y(x, 0))^2 dx + 2 \int_{\mathbb{R}^n} \kappa(x) (y(x, 0))^2 dx \\ &\leq 2T^2 \|f\|_{1;\rho}^2 + 2 \|\sqrt{\kappa} f\|_{L^2(\mathbb{R}^n)}^2. \end{aligned}$$

This together with equation (2.4) shows the assertion. \square

Now, we prove boundedness of L :

Theorem 2.2. *The operator $L : H_0^1(\Omega) \rightarrow L^2(\Sigma)$ is bounded and*

$$\|L\| \leq \frac{\mathcal{C}_y \mathcal{C}(T) \sqrt{T}}{\sqrt{\min\{\kappa_{\min}, \rho_{\max}^{-1}\}}}. \quad (2.6)$$

Proof. For given f let y be the solution of equation (1.1). From equation (2.2) it follows that the solution y of equation (2.5) is in $H^1(\mathbb{R}^n)$ for every $t > 0$. Thus from equation (1.7) and equation (2.5) it follows that

$$\|y\|_{L^2(\Sigma)}^2 = \int_0^T \int_{\partial\Omega} y^2(t) dS(x) dt \leq \mathcal{C}_y^2 \int_0^T \|y(t)\|_1^2 dt \leq \frac{\mathcal{C}_y^2 \mathcal{C}(T)^2 T \|f\|_{1;\kappa,\rho}^2}{\min\{\kappa_{\min}, \rho_{\max}^{-1}\}}. \quad \square$$

Remark 2.3. From [23, Theorem 1] it follows that the trace $L[f]$ is in fact in $H_{\text{loc}}^{3/4}(\partial\Omega \times (0, T))$. Therefore, by finite speed of propagation (Theorem 2.8), if we in addition assume that f is supported away from $\partial\Omega$, $L[f]$ is in fact in $H^{3/4}(\partial\Omega \times (0, T))$. The proof does not follow in a straightforward way from standard trace results, but utilizes the theory of Fourier integral operators and microlocal analysis. In special cases, this result can be further improved, see [21, Remark 5] and also [4, 5]. For instance, for Ω strictly convex, we have $L[f] \in H^1(\partial\Omega \times (0, T))$. As a consequence, $L : H_0^1(\Omega) \rightarrow L^2(\Sigma)$ is compact (see e.g. [3, Theorem 2.34]).

In the following we characterize the adjoint of $L : H_0^1(\Omega) \rightarrow L^2(\Sigma)$ on a dense subset of $L^2(\Sigma)$. Since the operator $L^* : L^2(\Sigma) \rightarrow H_0^1(\Omega)$ is bounded (in fact, $\|L\| = \|L^*\|$), a characterization follows by limits of convergent sequences on dense subsets. Here we characterize L^* on $C_0^\infty(\Sigma)$ first and extend it by convergent sequences to $L^2(\Sigma)$.

Definition 2.4. Let i be the embedding operator from $H_0^1(\Omega)$ to $L^2(\Omega)$. Then $i^* : L^2(\Omega) \rightarrow H_0^1(\Omega)$ is the operator which maps a function $\psi \in L^2(\Omega)$ onto the solution of the equation

$$Du = \psi \quad \text{in } \Omega, \quad u = 0 \quad \text{on } \partial\Omega, \quad (2.7)$$

with $D := \kappa - \nabla \cdot \rho^{-1} \nabla$. In other words $i^* = D^{-1}$.

In the following we derive the adjoint L^* of the operator L , which is required for the implementation of the Landweber iteration below, on a dense subset of $L^2(\Sigma)$. The boundedness of L^* is guaranteed by elementary Hilbert space theory. Therefore, we get a characterization on $L^2(\Sigma)$ by limits of convergent sequences.

Theorem 2.5. For $h \in C_0^\infty(\Sigma)$ the adjoint of the operator L , defined in (2.1), is given by

$$L^*[h] = i^* \circ L_D^*[h], \quad (2.8)$$

where

$$L_D^*[h] = \kappa z'(0)|_\Omega, \quad (2.9)$$

and $z := z(h)$ is the weak solution of

$$\begin{aligned} \kappa z'' - \nabla \cdot (\rho^{-1} \nabla z) &= 0 \quad \text{in } \mathbb{R}^n \setminus \partial\Omega \times (0, T), \\ z(T) = z'(T) &= 0 \quad \text{in } \mathbb{R}^n, \\ [z] = 0, \quad \left[\frac{\partial z}{\partial \mathbf{n}} \right] &= h \quad \text{on } \Sigma, \\ [z] = 0, \quad \left[\frac{\partial z}{\partial \mathbf{n}} \right] &= 0 \quad \text{on } \partial\Omega \setminus \Sigma \times (0, T). \end{aligned} \quad (2.10)$$

Here

$$[z] := z^+|_\Sigma - z^-|_\Sigma \quad \text{and} \quad \left[\frac{\partial z}{\partial \mathbf{n}} \right] := \frac{\partial z^+}{\partial \mathbf{n}} \Big|_\Sigma - \frac{\partial z^-}{\partial \mathbf{n}} \Big|_\Sigma,$$

where $z^+ := z|_{C\Omega \times (0, T)}$ and $z^- := z|_{\Omega \times (0, T)}$.

Proof. The existence of a weak solution of equation (2.10) is analogous to [6, Appendix A], where the transmission problem has been studied for variable sound speed. Multiplying the first equation of equation (2.10) by the solution of equation (1.1) y , it follows that $h \in C_0^\infty(\Sigma)$:

$$\int_\Sigma hL[f] dS(x) dt = \int_\Sigma hy dS(x) dt = \int_\Omega \kappa z'(0)f dx = \int_\Omega D[D^{-1}[\kappa z'(0)]]f dx = \langle i^*[\kappa z'(0)], f \rangle_{1;\kappa,\rho}. \quad \square$$

The following results on finite speed of propagation of the solution of equation (1.1) are based on the results from [9].

Definition 2.6. Let $d(x) := \text{dist}(x_0, x)$ be the distance between x_0 and x with respect to the Riemannian metric $\kappa\rho dx$. Note that this metric is chosen in accordance with the principal symbol of the elliptic operator $-\kappa^{-1}\nabla \cdot (\rho^{-1}\nabla \cdot)$. The cone \mathcal{K} with respect to the space-time point (t_0, x_0) is defined as

$$\mathcal{K} := \{(x, t) : d(x) < t_0 - t\}.$$

we further introduce

$$\mathcal{K}_t := \{x : d(x) < t_0 - t\},$$

the cross-section of \mathcal{K} at fixed time t .

Remark 2.7. According to [9, p. 416] the function d solves the PDE

$$\frac{1}{\rho\kappa} |\nabla d|^2 = 1, \quad d(x_0) = 0. \quad (2.11)$$

This relation will be used in the proof of Theorem 2.8 below.

Theorem 2.8. *Let y be the solution of equation (1.1). Assume $y' \equiv 0$ on \mathcal{K}_0 . Then $y \equiv 0$ in \mathcal{K} .*

Proof. Let

$$E_{\mathcal{K}_t}(t; y) := \frac{1}{2} \int_{\mathcal{K}_t} \kappa y'^2 + \rho^{-1} |\nabla y|^2 dx \quad (2.12)$$

denote the local energy. Taking the time derivative of $E_{\mathcal{K}_t}$, it follows by application of the Leibniz rule for the differentiation of evolving region integrals [9, p.713] that

$$E'_{\mathcal{K}_t}(t; y) = \int_{\mathcal{K}_t} \kappa y' y'' + \rho^{-1} \nabla y \cdot \nabla y' dy + \frac{1}{2} \int_{\partial \mathcal{K}_t} (\kappa y'^2 + \rho^{-1} |\nabla y|^2) \mathbf{v} \cdot \mathbf{n} dS(x),$$

where \mathbf{v} denotes the normal velocity of the moving boundary $\partial \mathcal{K}_t$ and \mathbf{n} is the outward pointing unit normal to \mathcal{K}_t . For a fixed point $x \in \mathcal{K}_t$, we have $\mathbf{v}(x) = \frac{\nabla d(x)}{|\nabla d(x)|^2}$ and $\mathbf{n}(x) = -\frac{\nabla d(x)}{|\nabla d(x)|}$. Therefore,

$$E'_{\mathcal{K}_t}(t; y) = \int_{\mathcal{K}_t} \kappa y' y'' + \rho^{-1} \nabla y \cdot \nabla y' dy - \frac{1}{2} \int_{\partial \mathcal{K}_t} (\kappa y'^2 + \rho^{-1} |\nabla y|^2) \frac{1}{|\nabla d|} dS(x) =: A - B. \quad (2.13)$$

By application of Green's formula, A is rewritten to

$$A = \int_{\mathcal{K}_t} y' (\kappa y'' - \nabla \cdot (\rho^{-1} \nabla y)) dx + \int_{\partial \mathcal{K}_t} \rho^{-1} y' \nabla y \cdot \frac{\nabla d}{|\nabla d|} dS(x).$$

The first term vanishes since y is solution to equation (1.1) and thus from equation (2.11) it follows that

$$|A| \leq \int_{\partial \mathcal{K}_t} \frac{|y'| \rho^{-1/2} |\nabla d| |\nabla y| \rho^{-1/2}}{|\nabla d|} dS(x) = \int_{\partial \mathcal{K}_t} \frac{|y'| \kappa^{1/2} |\nabla y| \rho^{-1/2}}{|\nabla d|} dS(x).$$

Using Cauchy's inequality, we finally obtain

$$|A| \leq \frac{1}{2} \int_{\partial \mathcal{K}_t} (\kappa y'^2 + \rho^{-1} |\nabla y|^2) \frac{1}{|\nabla d|} dS(x) = B.$$

Thus, from equation (2.13) it follows that $E'_{\mathcal{K}_t}(t; y) \leq 0$. □

3 Photoacoustic imaging

The *photoacoustic imaging problem* can be expressed as the solution of the operator equation

$$L[f] = m. \quad (3.1)$$

Uniqueness of the solution of equation (3.1) is closely related to a unique continuation result for the wave equation:

Theorem 3.1 (Unique Continuation, [12, 20, 22]). *Let u be a solution to equation (1.1), and assume that $y \equiv 0$ in $(-T, T) \times B_\varepsilon(x_0)$. Then*

$$y \equiv 0 \quad \text{in } \{(x, t) \in \mathbb{R} \times \mathbb{R}^n : \text{dist}(x, x_0) \leq T - |t|\}.$$

Uniqueness of the solution of equation (3.1) requires a sufficiently large observation time

$$T_0 := \max_{x \in \text{supp } f} \text{dist}(x, S), \quad (3.2)$$

where $\text{dist}(x, S)$ is the distance of x to the closest point $x' \in S$ with respect to the Riemannian metric $\kappa \rho dx$.

Corollary 3.2 (Injectivity of L , [21]). *Let Ω be strictly convex and $T > T_0$. Moreover, let $\text{supp } f \subset \Omega$. Then $L[f] = 0$ implies $f = 0$.*

In the following we discuss several numerical algorithms for solving equation (3.1).

3.1 Landweber iteration

We are employing the Landweber's iteration for solving equation (3.1) and compare it with the time reversal methods presented in Section 3.2, which are the standard references in this field. More efficient iterative regularization algorithms are at hand [11], but these are less intuitive to be compared with time reversal. The Landweber algorithm reads as follows:

$$f_0 := 0 \quad \text{and} \quad f_k^\delta = f_{k-1}^\delta - \omega L^* [L[f_{k-1}^\delta] - m^\delta], \quad k = 1, 2, \dots, \quad (3.3)$$

where m^δ stands for error-prone data with $\|m^\delta - m\|_{L^2(\Sigma)} < \delta$, where $m = y|_\Sigma$. For a summary of results for Landweber regularization in Photoacoustics we refer to [6] and the references therein.

We emphasize that Landweber's iteration converges to the *minimum norm solution*

$$f^\dagger = L^\dagger[m], \quad (3.4)$$

where L^\dagger is the Moore–Penrose inverse (see [18] for a survey), if the data m is an element of the range of L . This is a property which is relevant when the observation time T is smaller than the critical time T_0 which guarantees injectivity of L .

3.2 Time reversal

In this subsection, we first state the conventional time reversal and give a remark on necessary assumptions to obtain error estimates for this method. This is followed by a description of a modified time reversal approach, for which a theoretical analysis based on [21] can be provided.

3.2.1 Conventional time reversal

We formally define the time reversal operator

$$\bar{L}[h] = z(\cdot, 0), \quad (3.5)$$

where z is a solution of

$$\begin{aligned} \kappa z'' - \nabla \cdot (\rho^{-1} \nabla z) &= 0 & \text{in } \Omega \times (0, T), \\ z(T) = z'(T) &= 0 & \text{in } \Omega, \\ z &= h & \text{on } \partial\Omega \times (0, T). \end{aligned} \quad (3.6)$$

The fundamental difference between \bar{L} and L^* is that they are defined via differential equations on $\Omega \times (0, T)$ and $\mathbb{R}^n \times (0, T)$. The conventional time reversal reconstruction [25] consists of computing

$$f_{\text{TR}} = \bar{L}[m]. \quad (3.7)$$

Remark 3.3. Assume that $S = \partial\Omega$, that $\rho \equiv 1$ and the speed of sound is non-trapping. For this case, Hristova [13, Theorem 2] provides an error estimate for the time reversal method, employing results on the decay of solutions of the wave equation (e.g. [27]).

3.2.2 Neumann series

Stefanov and Uhlmann [21] define the modified time reversal for equation (1.1): Rather than assuming (in most cases unjustified) the initial data $z(T) \equiv 0$ we are again using the harmonic extension of the data term $h(s, T)$, for $s \in \partial\Omega$, as initial datum at T . That is, for

$$-\nabla \cdot (\rho^{-1} \nabla \phi) = 0 \quad \text{in } \Omega \quad \text{with} \quad \phi(\cdot) = m(\cdot, T) \quad \text{on } \partial\Omega$$

the modified time reversal operator

$$\widetilde{L}[h] = z(\cdot, 0) \quad (3.8)$$

is defined by the solution of equation

$$\begin{aligned} \kappa z'' - \nabla \cdot (\rho^{-1} z) &= 0 && \text{in } \Omega \times (0, T), \\ z(T) = \phi, \quad z'(T) &= 0 && \text{in } \Omega, \\ z &= h && \text{on } \partial\Omega \times (0, T). \end{aligned} \quad (3.9)$$

Note that this algorithm has not been used as a basis for numerical reconstruction for the generalized equation (1.1).

Previously [21] showed stability of the modified time reversal reconstruction under non-trapping conditions and for sufficiently large measurement time for equation (1.2). In fact, let $c = (\kappa\rho)^{-1/2}$ be non-trapping [14] and T_1 denote the time when all singularities have left $\overline{\Omega}$. Then the result is directly convertible to equation (1.1):

Theorem 3.4 (Stability of Modified Time Reversal, [21, Theorem 1]). *Let $T > T_1$ and let $S = \partial\Omega$ be a closed C^2 -surface. Moreover, let the coefficients $\kappa, \rho \in C^\infty(\mathbb{R}^n)$. Then $\widetilde{L}L = \text{Id} - K$, where K is a compact operator from $H_0^1(\Omega) \rightarrow H_0^1(\Omega)$ satisfying $\|K\| < 1$.*

Note that [21, Theorem 1] works only for complete boundary measurement data.

By Theorem 3.4, the initial value f can be expanded into the Neumann series

$$f = \sum_{j=0}^{\infty} K^j[m]. \quad (3.10)$$

By induction one sees that the m -th iterate can be written as

$$f_k = f_{k-1} - \widetilde{L}[L[f_{k-1}] - m], \quad (3.11)$$

where

$$f_k = \sum_{j=0}^k K^j[m].$$

Remark 3.5. Note that with partial data, the Neumann series reconstruction consists in formally applying equation (3.10) to the extended data m_s , where

$$m_s = m \quad \text{in } \Sigma' \subset\subset \Sigma \quad \text{and} \quad m_s = 0 \quad \text{in } \partial\Omega \setminus \Sigma \times (0, T), \quad (3.12)$$

in a way that $m_s \in H^1(\partial\Omega \times [0, T])$ serves as approximation to m in Σ .

Let now $S \subset \partial\Omega$ relatively open. To fix the terminology, we define for $(x, \xi) \in \mathbb{R}^n \times \mathbb{S}^{n-1}$ the curve $\gamma_{(x, \xi)}(\tau)$ to be the geodesic (in the Riemannian metric $\kappa\rho dx$) through x in direction ξ , where $\tau \in (-\infty, \infty)$ and $\gamma_{(x, \xi)}(0) = x$. Note that

$$\tau_{\pm}(x, \xi) = \max\{\tau \geq 0 : \gamma_{(x, \xi)}(\pm\tau) \in \overline{\Omega}\}$$

give the (possibly infinite) times when the geodesics leave the domain in positive ($\text{sgn} = +$) respectively negative ($\text{sgn} = -$) direction. Regarding stability [21, Theorem 3] provides the following result, which holds also in the partial data case.

Theorem 3.6. *Assume that $(\tau_{\text{sgn}}(x, \xi), \gamma_{(x, \xi)}(\tau_{\text{sgn}}(x, \xi))) \in \Sigma$ holds for all $(x, \xi) \in \Omega_1 \times \mathbb{S}^{n-1}$ in at least one of the two directions $\text{sgn} = +, \text{sgn} = -$. Then there exists a constant $C > 0$ such that for any $f \in C_0^\infty(\Omega_1)$, with $\Omega_1 \subset\subset \Omega$, the estimate*

$$\|f\|_{H_0^1(\Omega_1)} \leq C \|Lf\|_{H^1(\Sigma)}$$

is valid.

4 Numerical experiments and results

We compare conventional time reversal equation (3.7), the Neumann series approach equation (3.11) and the Landweber iteration equation (3.3) for the photoacoustic imaging problem based on equation (1.1). Similar studies have been performed in [6] for photoacoustic imaging based on equation (1.2). Figure 1 displays the involved parameters, including absorption density f , material compressibility κ and density ρ .

For the numerical solution of the involved wave equations equation (1.1) and equation (2.10), we use a straight-forward adaptation of the BEM-FEM scheme outlined in [6]. equation (3.6) and equation (3.9) are discretized by finite element discretization.

For the simulation of the data, for all different wave equations, the mesh size has been chosen as $\Delta x = 0.0095$ and $\Delta t = \Delta x / (15 * c_{\max})$, leading to about 40000 nodal points in Ω . For all wave equations involved in reconstruction, we use a grid with $\Delta x_R = 0.01$ and $\Delta t_R = \Delta x_R / (15 * c_{\max})$.

Measurement data are assumed to be recorded on 630 detection points on the unit circle. In the partial data example, the measurements are restricted to the lower half of the circle.

The total measurement time was varied as multiples of T_0 , which is defined as in equation (3.2).

4.1 Test Example 1 – Reconstruction from either noisy or partial data

We investigate the performance of the different photoacoustic imaging techniques, time reversal, Neumann series and Landweber iteration, respectively, with spatially varying κ and ρ . We show different test cases

- for partial measurement data (see Figure 2), where we show the imaging results for $T = 2T_0$ and $T = 4T_0$, where T_0 , defined in equation (3.2), denotes the minimal time that guarantees unique reconstruction of the absorption density f ,
- as well as reconstructions from full data in the presence of noise (Figure 3). The noise level is stated as SNR (signal to noise ratio, in dB scale) with respect to the maximum signal value. The examples include moderate noise (SNR = 10 dB) and high noise (SNR = 5 dB).

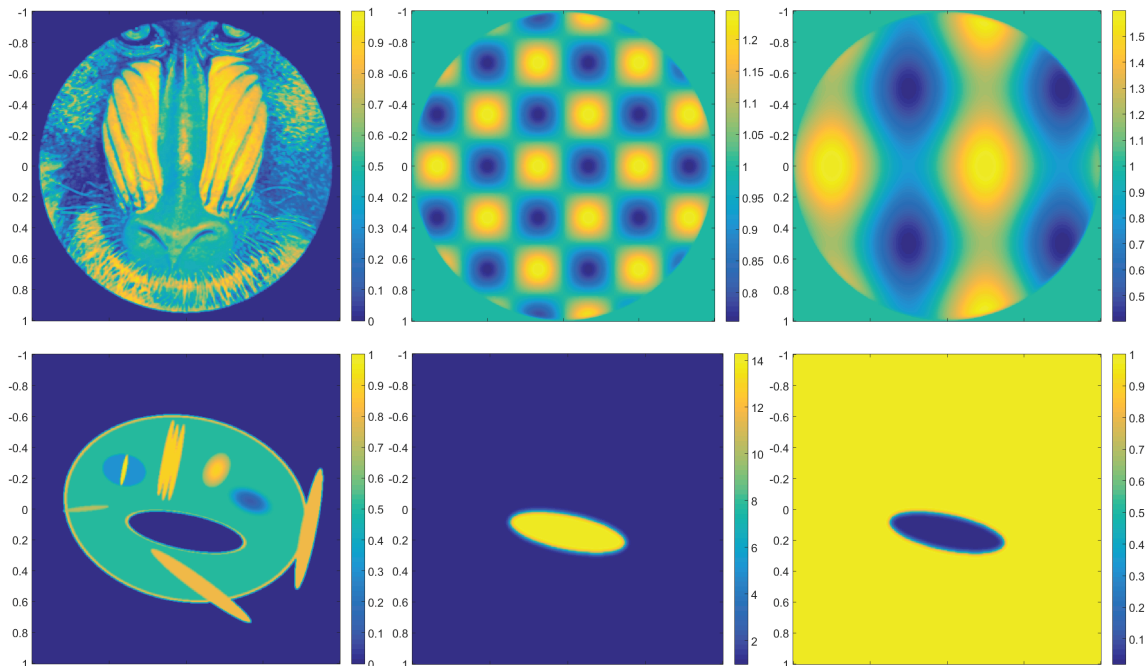


Figure 1. Parameters: **First row:** Test Example 1 – *Mandrill*. **Second row:** Test Example 2 – *Fish*. **From left to right:** initial pressure f , compressibility κ , density ρ .

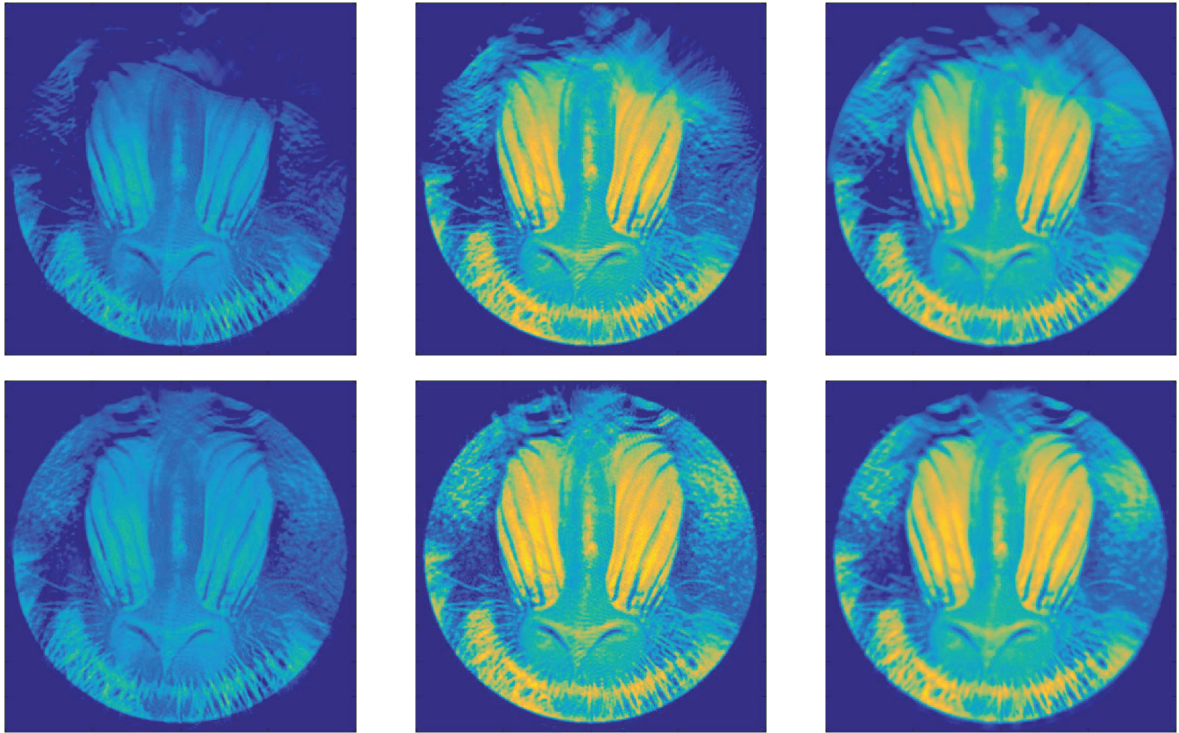


Figure 2. Partial data reconstructions: Data are recorded on the lower unit half-circle and the parameters κ, ρ are exactly given. Data are noise free and recorded for $T = 2T_0, 4T_0$. Reconstructions for $T = 2T_0, 4T_0$ are shown in the first and second row, respectively. **From left to right:** time reversal, Neumann series with $k = 5$, Landweber iterate $k = 5$.

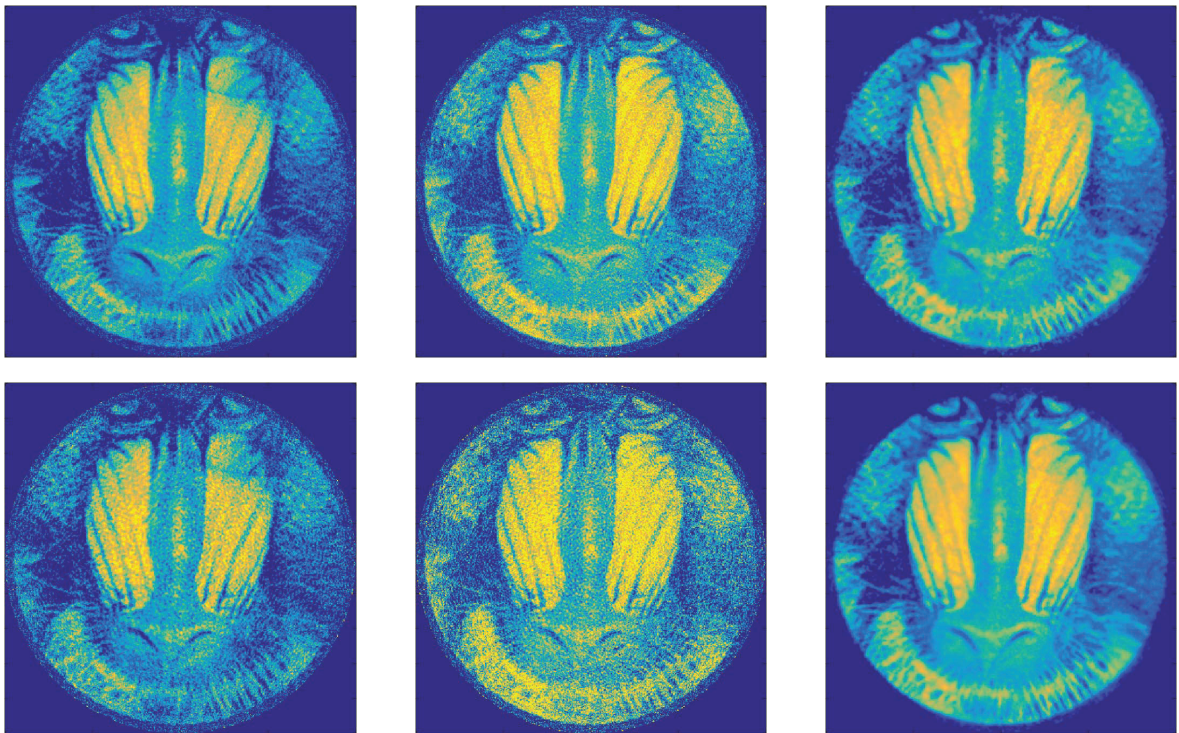


Figure 3. Reconstruction with complete, but noisy measurements and correct parameters κ, ρ , measurement time $T = 2T_0$. **First row:** SNR = 10 dB. **Second row:** SNR = 5 dB. **From left to right:** time reversal, Neumann series with $k = 5$, Landweber iterate $k = 5$.

4.2 Test Example 2 – Effect of modeling errors on reconstruction

The second test concerns a parameter setting κ, ρ and associated sound speed $c = (\kappa\rho)^{-1/2}$, which is reconstructed with inversions (time reversal, Neumann series, Landweber iteration) based on equation (1.2) and equation (1.3). This results in a modeling error, whose effect depends on the magnitude of the gradient of ρ , respectively κ .

First, we use the *Mandrill* phantom and according acoustic parameters from Section 4.1. Here, the maximum gradient magnitude of the density and compressibility functions is relatively small. In addition, the initial pressure given by the Mandrill phantom does not show too large gradients as well. By employing equation (2.4), we can thus argue that the second term on the right-hand side in $\nabla \cdot (\rho^{-1}\nabla y) = \rho^{-1}\Delta y + \nabla\rho^{-1} \cdot \nabla y$ is negligible. A similar argument gives a justification for the approximation by equation (1.3).

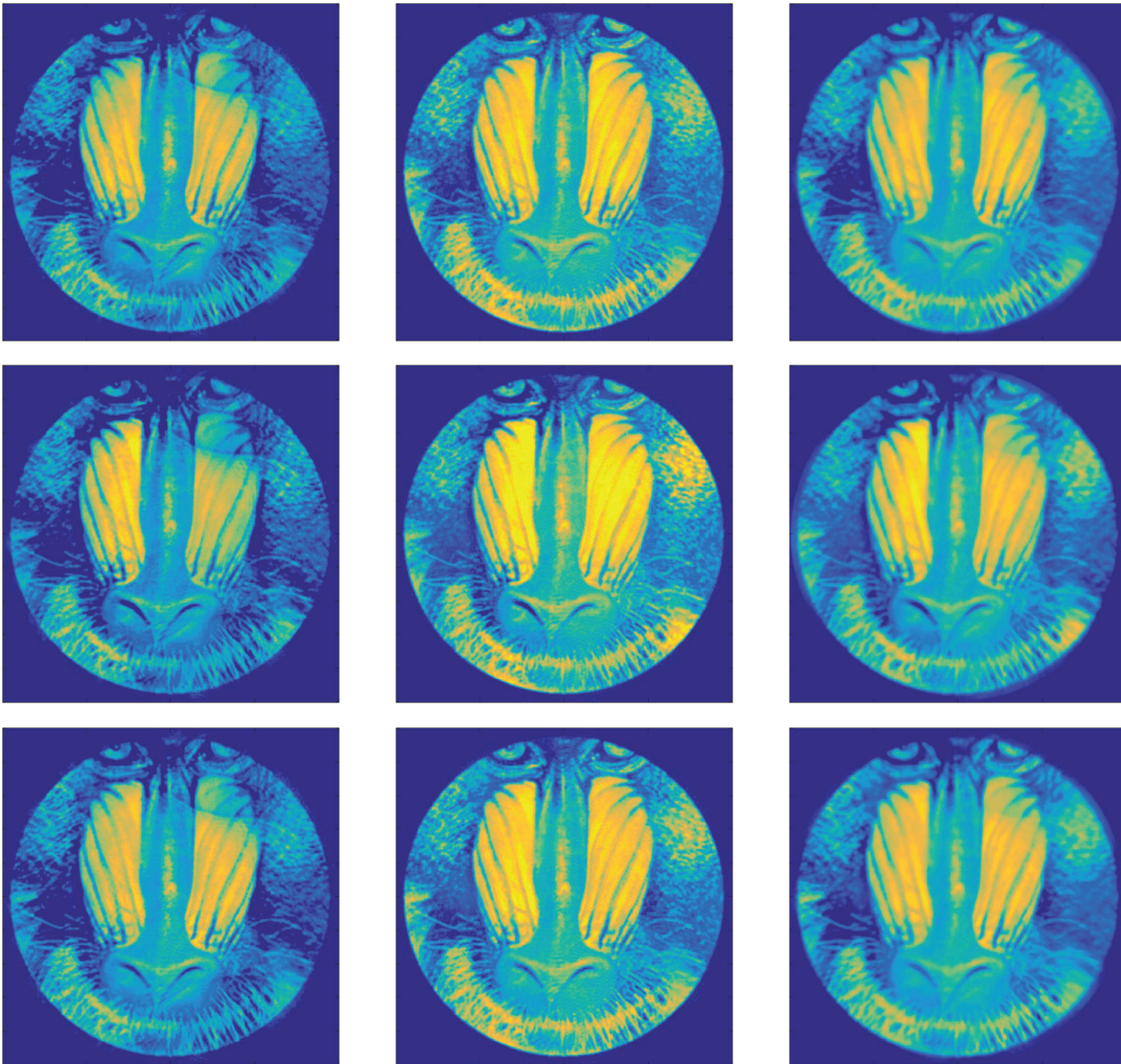


Figure 4. Reconstructions of the *Mandrill* phantom with $T = 2T_0$. **First row:** Reconstruction using correct parameters $\kappa_1 = \kappa$, $\rho_1 = \rho$ as pictured in the second row of Figure 1. **Second row:** Reconstruction with parameters $\kappa_1 = \kappa\rho$, $\rho_1 \equiv 1$. **Third row:** Reconstruction with parameters $\rho_1 = \kappa\rho$, $\kappa_1 \equiv 1$. **From left to right:** Time reversal, Neumann series with $k = 5$, Landweber iterate $k = 5$.

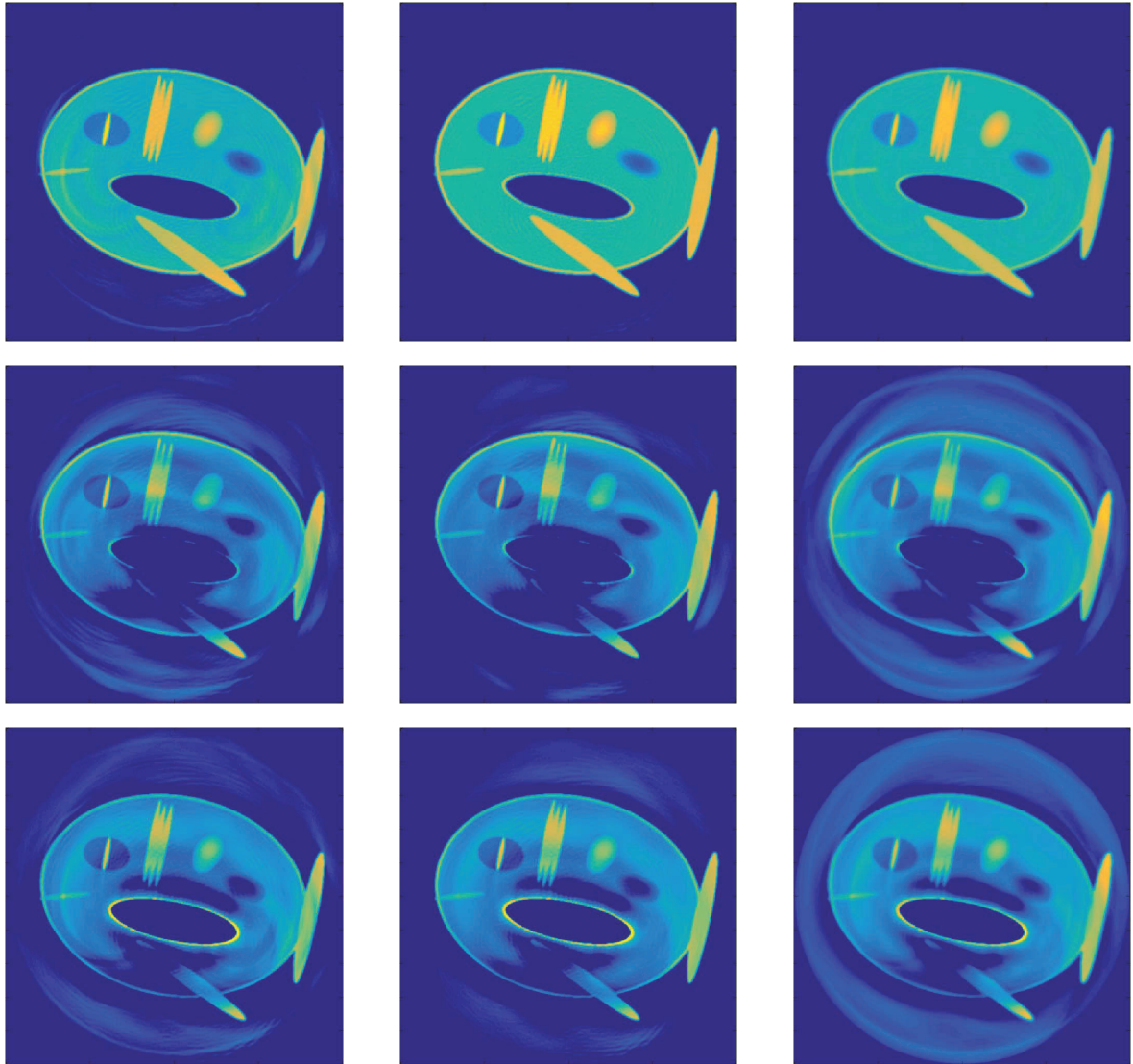


Figure 5. Reconstructions of the *Fish* phantom with $T = 2T_0$. **First row:** Reconstruction using correct parameters $\kappa_1 = \kappa$, $\rho_1 = \rho$ as pictured in the second row of Figure 1. **Second row:** Reconstruction with parameters $\kappa_1 = \kappa\rho$, $\rho_1 \equiv 1$. **Third row:** Reconstruction with parameters $\rho_1 = \kappa\rho$, $\kappa_1 \equiv 1$. **From left to right:** Time reversal, Neumann series with $k = 5$, Landweber iterate $k = 5$.

The second phantom simulates a water-like body (e.g. soft tissue) containing an inclusion with significantly different acoustic properties, like the air-filled swim-bladder of a fish (see lower row of Figure 1). We choose the parameters to be bounded in the intervals $0.02 \leq \rho \leq 1$ and $1 \leq \kappa \leq 14.3$, with high gradients in the transition between the inclusion and the rest of the domain (see also Figure 1).

Moreover, we include the achievable results when only $c = (\kappa\rho)^{-1/2}$ is known, leading to a modeling error in the reconstructions.

- In the first row of Figure 4, respectively Figure 5, we display the reconstructions with correct parameters κ, ρ as depicted in the second row of Figure 1.
- Next, reconstructions are performed by using the parameters $\kappa_1 = \kappa\rho$ and $\rho_1 = 1$, which now play the role of κ and ρ in (1.1). This is equivalent to the usually considered approximation given by equation (1.2) (see second row of Figure 4, Figure 5).
- We also try it the other way round by setting $\rho_2 = \kappa\rho$, and $\kappa_2 \equiv 1$ (third row of Figure 4, Figure 5). This leads to the wave equation in pure divergence form, and displays the case where the compressibility variations are negligible.

As mentioned above, the visible error obtained by the approximations in (b) and (c) depends on the gradient magnitude of the given parameters f, κ, ρ . The results are discussed in Section 4.

4.3 Results

In the presented test examples, all three methods qualitatively reconstruct the same features. Time reversal however fails to give quantitatively correct results, due to the relatively short measurement times in use (a more detailed comparison of the performance of time reversal relative to the reconstruction time can be found in [6]). Neumann series and Landweber iteration perform at a comparable level. As expected from theory, the Landweber reconstructions appear slightly smoother, specifically in Figure 3, whereas the noise is amplified in the Neumann series approach. In the case of partial data, there is no theoretical convergence result for the Neumann series approach available (note, however, Theorem 3.6), whereas Landweber converges to the minimum norm solution (see Section 3.1, Section 5 and Table 1).

The second test clearly indicates that a modeling error in the reconstruction method can lead to severe artifacts near regions where the magnitude of the parameter gradient is large. However, in cases where the parameters are relatively slowly varying, the modeling error is negligible, as it is displayed in Figure 4.

5 Conclusions

In this work we have studied photoacoustic imaging based on a general wave model with spatially variable compressibility and density, respectively. We have implemented Neumann series and Landweber iteration for photoacoustic imaging based on this general equation and we compared the result to conventional time reversal as discussed in [25].

The numerical methods for photoacoustic imaging reveal the differences as outlined in Table 1 with respect to convergence, stability and robustness against noise at the present stage of research. Stability is understood in the sense of regularization theory [10], meaning that the Landweber iterates determined by a discrepancy principle approximate the minimum norm solution.

Numerical results show the reconstructions in the case of error prone data and under modeling errors. We emphasize that, so far, an error analysis is only possible for the Landweber iteration.

	Time reversal	Neumann	Landweber
Convergence			best approximate solution
measurement time	$T \rightarrow \infty$	$T > T_1$	$T > 0$
sound speed	non-trapping	non-trapping	arbitrary
data	full	full	partial
Stability			regularized solution
measurement time	$T > T_1$	$T > T_1/2$	$T > 0$
sound speed	non-trapping	non-trapping	arbitrary
data	full	partial	partial
L^2 -noise	no	no	yes

Table 1. Overview on the different photoacoustic imaging methods.

Acknowledgment: We are grateful to the valuable hints of Silvia Falletta concerning details to discretization and implementation of the coupled FEM-BEM system.

Funding: The work of Thomas Glatz and Otmar Scherzer is supported by the Austrian Science Fund (FWF), Project P26687-N25 Interdisciplinary Coupled Physics Imaging.

References

- [1] R. A. Adams, *Sobolev Spaces*, Academic Press, New York, 1975.
- [2] M. Agranovsky and P. Kuchment, Uniqueness of reconstruction and an inversion procedure for thermoacoustic and photoacoustic tomography with variable sound speed, *Inverse Problems* **23** (2007), no. 5, 2089–2102.
- [3] T. Aubin, *Nonlinear Analysis on Manifolds, Monge–Ampère Equations*, Grundlehren Math. Wiss. 252, Springer, Berlin, 1982.
- [4] G. Bao and W. W. Symes, A trace theorem for solutions of partial differential equations, *Math. Methods Appl. Sci.* **14** (1991), no. 8, 553–562.
- [5] G. Bao and W. W. Symes, Trace regularity for a second order hyperbolic equation with non-smooth coefficients, *J. Math. Anal. Appl.* **174** (1993), 370–389.
- [6] Z. Belhachmi, T. Glatz and O. Scherzer, A direct method for photoacoustic tomography with inhomogeneous sound speed, *Inverse Problems* **32** (2016), no. 4, Article ID 045005.
- [7] D. Colton and R. Kress, *Inverse Acoustic and Electromagnetic Scattering Theory*, Appl. Math. Sci. 93, Springer, Berlin, 1992.
- [8] H. W. Engl, M. Hanke and A. Neubauer, *Regularization of Inverse Problems*, Math. Appl. 375, Kluwer Academic Publishers, Dordrecht, 1996.
- [9] L. C. Evans, *Partial Differential Equations*, 2nd ed., Grad. Stud. Math. 19, American Mathematical Society, Providence, 2010.
- [10] C. W. Groetsch, *The Theory of Tikhonov Regularization for Fredholm Equations of the First Kind*, Pitman, Boston, 1984.
- [11] M. Hanke, *Conjugate Gradient Type Methods for Ill-Posed Problems*, Pitman Res. Notes in Math. 327, Longman Scientific & Technical, Harlow, 1995.
- [12] L. Hörmander, A uniqueness theorem for second order hyperbolic differential equations, *Comm. Partial Differential Equations* **17** (1992), 699–714.
- [13] Y. Hristova, Time reversal in thermoacoustic tomography—An error estimate, *Inverse Problems* **25** (2009), no. 5, Article ID 055008.
- [14] Y. Hristova, P. Kuchment and L. Nguyen, Reconstruction and time reversal in thermoacoustic tomography in acoustically homogeneous and inhomogeneous media, *Inverse Problems* **24** (2008), no. 5, Article ID 055006.
- [15] C. Huang, L. Nie, R. W. Schoonover, L. Wang and M. A. Anastasio, Photoacoustic computed tomography correcting for heterogeneity and attenuation, *J. Biomed. Opt.* **17** (2012), Article ID 061211.
- [16] P. Kuchment, *The Radon Transform and Medical Imaging*, Society for Industrial and Applied Mathematics, Philadelphia, 2014.
- [17] P. Kuchment and L. Kunyansky, Mathematics of thermoacoustic tomography, *European J. Appl. Math.* **19** (2008), 191–224.
- [18] M. Nashed, *Generalized Inverses and Applications*, Academic Press, New York, 1976.
- [19] J. Qia, P. Stefanov, G. Uhlmann and H. Zhao, An efficient Neumann series-based algorithm for thermoacoustic and photoacoustic tomography with variable sound speed, *SIAM J. Imaging Sci.* **4** (2011), no. 3, 850–883.
- [20] L. Robbiano, Théorème d’unicité adapté au contrôle des solutions des problèmes hyperboliques, *Comm. Partial Differential Equations* **16** (1991), no. 4–5, 789–800.
- [21] P. Stefanov and G. Uhlmann, Thermoacoustic tomography with variable sound speed, *Inverse Problems* **25** (2009), no. 7, Article ID 075011.
- [22] D. Tataru, Unique continuation for solutions to PDEs; between Hörmander’s theorem and Holmgren’s theorem, *Comm. Partial Differential Equations* **20** (1995), no. 5–6, 855–884.
- [23] D. Tataru, On the regularity of boundary traces for the wave equation, *Ann. Sc. Norm. Super. Pisa Cl. Sci. (4)* **26** (1998), no. 1, 185–206.
- [24] J. Tittelfitz, Thermoacoustic tomography in elastic media, *Inverse Problems* **28** (2012), no. 5, Article ID 055004.
- [25] B. E. Treeby and B. T. Cox, K-Wave: MATLAB toolbox for the simulation and reconstruction of photoacoustic wave fields, *J. Biomed. Opt.* **15** (2010), Article ID 021314.
- [26] B. E. Treeby, T. K. Varshney, E. Z. Zhang, J. G. Laufer and P. C. Beard, Automatic sound speed selection in photoacoustic image reconstruction using an autofocus approach, *J. Biomed. Opt.* **16** (2011), no. 9, 090501–3.
- [27] B. R. Vainberg, On the short wave asymptotic behaviour of solutions of stationary problems and the asymptotic behaviour as $t \rightarrow \infty$ of solutions of non-stationary problems, *Russian Math. Surveys* **30** (1975), no. 2, 1–58.
- [28] L. V. Wang, *Photoacoustic Imaging and Spectroscopy*, Opt. Sci. Eng., CRC Press, Boca Raton, 2009.
- [29] M. Xu and L. V. Wang, Exact frequency-domain reconstruction for thermoacoustic tomography—I: Planar geometry, *IEEE Trans. Med. Imaging* **21** (2002), no. 7, 823–828.
- [30] M. Xu and L. V. Wang, Time-domain reconstruction for thermoacoustic tomography in a spherical geometry, *IEEE Trans. Med. Imaging* **21** (2002), no. 7, 814–822.
- [31] M. Xu and L. V. Wang, Universal back-projection algorithm for photoacoustic computed tomography, *Phys. Rev. E Stat. Nonlin. Soft Matter Phys.* **71** (2005), no. 1, Article ID 016706.
- [32] M. Xu and L. V. Wang, Photoacoustic imaging in biomedicine, *Rev. Sci. Instr.* **77** (2006), no. 4, Article ID 041101.

- [33] M. Xu, Y. Xu and L. V. Wang, Time-domain reconstruction algorithms and numerical simulations for thermoacoustic tomography in various geometries, *IEEE Trans. Biomed. Eng.* **50** (2003), no. 9, 1086–1099.
- [34] Y. Xu, M. Xu and L. V. Wang, Exact frequency-domain reconstruction for thermoacoustic tomography – II: Cylindrical geometry, *IEEE Trans. Med. Imaging* **21** (2002), 829–833.